

Effect of Structural Variation on Photocurrent Efficiency in Alkyl-Substituted Porphyrin Solid-State Thin Layer Photocells

Marye Anne Fox,* Jennifer V. Grant, Dan Melamed, Tsukasa Torimoto, Chong-yang Liu, and Allen J. Bard*

Department of Chemistry and Biochemistry, The University of Texas at Austin, Austin, Texas 78712

Received July 11, 1997. Revised Manuscript Received May 5, 1998

Three structurally variant alkyl-substituted porphyrins [zinc(II) 2,3,7,8,12,13,17,18-octa-*n*-decylporphyrin **2**, metal(II) *meso*-5,10,15,20-tetra-*n*-undecylporphyrin **3** (metal = cobalt, copper, palladium, and zinc), and zinc(II) *meso*-5,10,15,20-tetrakis(phenoxy-*n*-nonyl)porphyrin **4**] exist as photoconductive insulators and produce significant short circuit photocurrent and open circuit photopotential when irradiated as solid thin films in an indium–tin oxide sandwich cell. Liquid crystalline phase stability, the identity of the inserted metal, and the nature of its supramolecular packing all influence the observed photoelectrochemical response. Porphyrin **2**, which has a stable liquid crystalline phase, produces higher steady-state photocurrents than do the corresponding *meso*-substituted porphyrins **3** and **4**, although liquid crystallinity is not an absolute requirement for observation of a photoresponse. Among porphyrins **3**, the zinc complex gave the highest steady-state photocurrent. When a phenyl ring orthogonal to the porphyrinic plane was present (as in **4**), the observed photovoltaic response was significantly diminished, probably because of difficulties in achieving effective close packing.

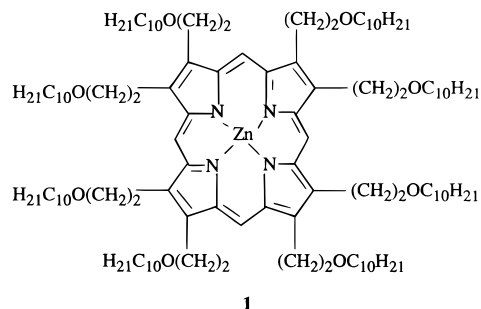
Introduction

Photovoltaic devices have numerous applications in photodetectors, switches, solar cells, and photodiodes,¹ and as the technology of molecular electronic devices evolves to produce faster, more efficient charge separation, the need for well-defined nanomaterials continues to increase. Thus, the ability to design materials with predetermined properties is a worthy, if elusive, goal.

Most practical semiconductor devices currently employ inorganic materials, largely because these materials can often be more easily fabricated as highly ordered crystals whose photovoltaic and electronic properties are generally superior in practical devices than ordered thin films or amorphous phases.^{2–4} Nevertheless, organic thin films are interesting for several reasons, including the versatility of their synthesis, their ease of processability, and their lower susceptibility to lattice impurities.

Porphyrins, phthalocyanines, and triphenylenes, in particular, have been found to be well-suited for such applications, especially those which exhibit stable liquid crystalline phases.^{5,6} For example, thin films of zinc

octakis(β -decoxyethyl)porphyrin **1** and its homologues



have been shown to exist as highly photoconductive insulators and to exhibit interesting photoelectrochemical properties, including appreciable short circuit photocurrents, significant open circuit photopotentials, and long-term charge storage when included as a solid thin layer in a symmetrical ITO sandwich cell.^{7–11} Given

(1) Streetman, B. G. *Solid State Electronic Devices*, 3rd ed.; Prentice Hall: Englewood Cliffs, NJ, 1990.

(2) Klofta, T. J.; Rieke, P. C.; Linkous, C. A.; Buttner, W. J.; Nanthakuma, A.; Mewborn, T. D.; Armstrong, N. R. *J. Electrochem. Soc.* **1985**, *132*, 2134.

(3) Law, K.-Y. *J. Phys. Chem.* **1988**, *92*, 4226.

(4) Hor, A. M.; Loutfy, R. O. *Thin Solid Films* **1983**, *106*, 291.

(5) (a) Simon, J.; Bassoul, P. In *Phthalocyanines: Properties and Applications*; Leznoff, C. C.; Lever, A. B. P., Eds.; VCH: New York, 1989; Vol. 2. (b) Simon, J. In *Nanostructures Based on Molecular Materials*; Göpel, W.; Zielger, Ch., Eds.; VCH: Weinheim, 1992.

(6) (a) Adam, D.; Schuhmacher, P.; Simmerer, J.; Haüssling, L.; Siemensmeyer, K.; Etbach, K. H.; Ringsdorf, H.; Haarer, D. *Nature* **1994**, *371*, 141. (b) Schouten, P. G.; Warman, J. M.; de Haas, M. P.; Fox, M. A.; Pan, H.-L. *Nature* **1991**, *353*, 736.

(7) (a) Gregg, B. A.; Fox, M. A.; Bard, A. J. *J. Phys. Chem.* **1990**, *94*, 1586. (b) Gregg, B. A.; Fox, M. A.; Bard, A. J. *J. Am. Chem. Soc.* **1989**, *111*, 3024.

(8) (a) Liu, C. Y.; Pan, H. L.; Fox, M. A.; Bard, A. J. *Science* **1993**, *261*, 897. (b) Liu, C. Y.; Pan, H. L.; Fox, M. A.; Bard, A. J. *Chem. Mater.* **1997**, in press. (c) Liu, C. Y.; Pan, H. L.; Tang, H.; Fox, M. A.; Bard, A. J. *J. Phys. Chem.* **1995**, *99*, 7632.

(9) Kugimiya, S.; Takemura, M. *Tetrahedron Lett.* **1990**, *31*, 3157.

(10) Simizu, Y.; Ishikawa, A.; Kusabayashi, S. *Chem. Lett.* **1986**, 1041.

the high stability of this family of aromatic porphyrins, their planar structure, and their facile π stacking, we wished to explore how structural variation within the family might affect photoconductivity and performance in a photovoltaic cell.

Seeking to provide an alternative to **1**, which requires a lengthy synthesis,⁸ we describe here the synthesis of the related porphyrins **2–4** and compare their photovoltaic properties with those of **1**. In addition, to probe the importance of supramolecular interactions to overall cell performance, we compare the photoresponses of the alkylated porphyrins **3** and **4**. Although we have found that neither of these compounds has a stable liquid crystalline phase, the nearly orthogonal phenyl rings¹² attached to the porphyrin at the meso positions in **4** should more significantly disrupt solid-state packing than in the meso-alkylated porphyrin **3**.

Experimental Section

Synthesis. Zinc(II) 2,3,7,8,12,13,17,18-Octa-*n*-decylporphyrin 2. In a dry 100 mL three-necked flask, 3,4-dibromo-1-(triisopropylsilyl)pyrrole^{13,14} (2.8 g, 7.2 mmol) was dissolved in THF (ca. 50 mL) and cooled to -78 °C. *n*-Butyllithium (1.6 M) in hexanes (5.0 mL, 8.0 mmol) was slowly added to the flask under Ar by addition funnel, at a rate to keep the temperature below -65 °C. After stirring for 20 min at -78 °C, iododecane (2.0 mL, 9.4 mmol) was added. The solution was warmed to -30 °C in a bromobenzene–liquid N₂ bath for 30 min and then cooled to -78 °C. *tert*-Butyllithium (1.6 M) in pentane (10.0 mL, 16.0 mmol) was added while the temperature was kept below -65 °C and the mixture stirred for 30 min, followed by the addition of iododecane (4.0 mL, 18.8 mmol). The resulting solution was then warmed to room temperature. The reaction mixture was washed with saturated NaHCO₃ (50 mL) and extracted with Et₂O (3 × 30 mL). The combined organic extracts were washed with saturated NaHCO₃, dried over MgSO₄, and filtered through silica using hexanes. The solvent was removed under reduced pressure to yield a red-brown oil. This oil was taken up in THF (ca. 50 mL) containing excess Bu₄NF·4H₂O (2.0 g, 7.6 mmol). The reaction mixture was stirred for 3 h, the solvent was removed under reduced pressure, and the residue was chromatographed on silica with hexanes followed by CH₂Cl₂ as the eluent. The solvent was removed under reduced pressure to yield a slightly impure dark brown oil (3,4-didecylpyrrole) which was used immediately without further purification. ¹H NMR (CDCl₃) δ 0.86 (t, 6 H, $J = 6.45$ Hz), 1.21 (m, 28 H), 1.45 (m, 4 H), 2.4 (t, 4 H, $J = 7.60$ Hz), 6.5 (d, 2 H, $J = 2.77$ Hz), 7.8 (s, 1 H).

Formaldehyde (0.50 mL of 30% aqueous solution) and *p*-toluenesulfonic acid (0.02 g) were added to a solution of 3,4-didecylpyrrole (3.6 g, 11 mmol) in benzene (ca. 250 mL). The solution was azeotropically distilled under N₂. After boiling for 12 h, the solution was bubbled with O₂ for 12 h and the solvent was removed under reduced pressure. The residue was chromatographed on silica by eluting with CH₂Cl₂ followed by hexanes and finally by 10:1 hexanes and ethyl acetate. The solvent was removed under reduced pressure and the resulting solid was dissolved in chloroform and treated with saturated methanolic Zn(OAc)₂. The resulting solution was heated to reflux and was then cooled to room temperature. The solid was recrystallized from chloroform and methanol to yield a deep burgandy solid (0.51 g, 0.34 mmol, 12%), mp 176–179

°C. (No attempt was made to optimize yield.) DSC for K–M, 117 °C, 4.5 kcal/mol; DSC for M–I, 177 °C, 2.1 kcal/mol; ¹H NMR (500 MHz, CDCl₃) δ 0.86 (t, 24 H, $J = 6.7$ Hz), 1.26 (m, 80 H), 1.55 (m, 16 H), 1.79 (m, 16 H), 2.29 (m, 16 H), 3.93 (m, 16 H), 9.90 (m, 4 H); ¹³C NMR (CDCl₃) δ 14.1, 22.7, 26.7, 29.4, 29.8, 29.9, 30.6, 32.0, 34.2, 97.7, 140.9, 147.5; HRMS C₁₀₀H₁₇₂N₄Zn calcd 1493.2873, found 1493.2894; UV (CHCl₃) λ_{\max} (log ϵ) 406 (5.4), 536 (4.2), 572 nm (4.3).

Metal(II) meso-5,10,15,20-Tetra-*n*-undecylporphyrins 3. Pyrrole (0.35 mL, 5.0 mmol) and dodecanal (1.1 mL, 5.0 mmol) were combined in 500 mL of chloroform. After purging the solution for 45 min with Ar, trifluoroacetic acid (0.20 mL) was added. The mixture was stirred under Ar in the absence of light for 25 h before DDQ (0.86 g, 3.8 mmol) was added. The solution was evaporated onto Fluorosil (ca. 10 g) and chromatographed using hexanes followed by 10:1 hexanes/ethyl acetate. The solvent was removed under reduced pressure to yield a slightly impure red-brown compound.

This free base porphyrin was dissolved in chloroform and heated to reflux under Ar, and 1 mL of saturated metal(II) salt in methanol was added. The solution was heated at reflux for 1 h before being cooled. The solvent was removed under reduced pressure, and the residue was chromatographed on silica with a 5% ethyl acetate in hexanes solution. The product was recrystallized from chloroform and methanol to yield a purple solid.

M = Zn (92 mg, 0.093 mmol, 7.4%); mp 128–131 °C; DSC for K–I, 131 °C, 9.9 kcal/mol; ¹H NMR (CDCl₃) δ 0.86 (t, 12 H, $J = 6.9$ Hz), 1.28 (m, 48 H), 1.54 (m, 8 H), 1.84 (m, 8 H), 2.52 (m, 8 H), 4.88 (t, 8 H, $J = 7.9$ Hz), 9.50 (s, 8 H); ¹³C NMR (CDCl₃) δ 14.1, 22.7, 29.4, 29.7, 29.8, 30.8, 31.9, 35.8, 39.0, 119.4, 128.9, 149.3; HRMS C₆₄H₁₀₀N₄Zn calcd 989.7345, found 989.7318; UV (CHCl₃) λ_{\max} (log ϵ) 424 (5.3), 558 (3.9), 602 nm (3.6).

M = Co. Metalation required 10 days at reflux (13 mg, 0.013 mmol, 3.1%) to yield a deep purple solid: mp 98–103 °C; DSC for K–I, 102 °C, 5.1 kcal/mol; HRMS C₆₄H₁₀₀N₄Co calcd 983.7280, found 983.7263; UV (CHCl₃) λ_{\max} (log ϵ) 414 (5.0), 542 nm (3.7).

M = Cu: Metalation required 24 h at reflux (71 mg, 0.072 mmol, 17%) to yield a deep purple solid: mp 104–107 °C; DSC for K–I, 106 °C, 10.6 kcal/mol; HRMS C₆₄H₁₀₀N₄Cu calcd 987.7237, found 987.7237; UV (CHCl₃) λ_{\max} (log ϵ) 420 (5.9), 548 (4.4), 584 nm (3.8).

M = Ni. Metalation required 48 h at reflux (68 mg, 0.069 mmol, 16%) to yield a red solid: dec 200 °C; DSC for K–I, 102 °C, 5.1 kcal/mol; ¹H NMR (CDCl₃) δ 0.84 (t, 12 H, $J = 6.6$ Hz), 1.21 (m, 48 H), 1.36 (m, 8 H), 1.51 (m, 8 H), 2.19 (m, 8 H), 4.44 (t, 8 H, $J = 7.9$ Hz), 9.20 (s, 8 H); ¹³C NMR (CDCl₃) δ 14.1, 22.7, 29.3, 29.6, 29.7, 30.3, 31.9, 33.9, 37.2, 116.8, 129.6, 141.1; HRMS C₆₄H₁₀₀N₄Ni calcd 982.7301, found 982.72711; UV (CHCl₃) λ_{\max} (log ϵ) 422 (5.6), 540 (4.3), 668 nm (3.0).

M = Pd. Metalation required 24 h at reflux (20 mg, 0.019 mmol, 5%) to yield a red solid: mp 79–82 °C; DSC for K–I, 81 °C, 7.0 kcal/mol; ¹H NMR (CDCl₃) δ 0.88 (t, 12 H, $J = 6.6$ Hz), 1.28 (m, 48 H), 1.51 (m, 8 H), 1.78 (m, 8 H), 2.46 (m, 8 H), 4.76 (t, 8 H, $J = 7.9$ Hz), 9.35 (s, 8 H); ¹³C NMR (CDCl₃) δ 14.1, 22.7, 29.4, 29.7, 30.0, 30.6, 31.9, 35.2, 38.3, 119.7, 127.9, 140.4; HRMS C₆₄H₁₀₀N₄Ni calcd 1030.6983, found 1030.6952; UV (CHCl₃) λ_{\max} (log ϵ) 420 (5.6), 532 (4.4), 564 nm (3.8).

Zinc(II) meso-5,10,15,20-Tetrakis(*p*-phenoxy-*n*-nonyl)porphyrin 4. Pyrrole (0.35 mL, 5.0 mmol) and 4-nonylbenzaldehyde (1.1 mL, 1.2 g, 5.0 mmol) were combined in 500 mL of chloroform in a dry 1000 mL round-bottom flask. After purging the solution for 1 h with Ar, trifluoroacetic acid (0.20 mL) was added. The mixture was stirred under Ar in the absence of light for 3 days before DDQ (0.86 g, 3.8 mmol) was added. After the solution was stirred for 1 h, it was evaporated onto Fluorosil (ca. 10 g) and chromatographed using hexanes followed by 10:1 hexanes and ethyl acetate as the eluent. The solvent was removed under reduced pressure and the residue was taken up in chloroform, heated to reflux, and treated with 1 mL of methanolic Zn(OAc)₂. After the solution was heated

(11) Shimizu, Y.; Ishikawa, A.; Kusabayashi, S.; Miya, M.; Nagata, A. *J. Chem. Soc., Chem. Commun.* **1993**, 656.

(12) Fleischer, E. B.; Miller, C. K.; Webb, L. E. *J. Am. Chem. Soc.* **1964**, *86*, 2342.

(13) Bray, B. L.; Mathies, P. H.; Naef, R.; Solas, D. R.; Tidwell, T. T.; Artis, D. R.; Muchowski, J. M. *J. Org. Chem.* **1990**, *55*, 6317.

(14) Shum, P. W.; Kozikowski, A. P. *Tetrahedron Lett.* **1990**, *31*, 6785.

to reflux for 1 h, it was cooled, the solvent removed, and the residue filtered through silica with 10:1 solution of hexanes and ethyl acetate. The resulting solid was recrystallized from chloroform and methanol to yield an iridescent purple solid (0.14 g, 0.11 mmol, 8.9%): mp 187–189 °C; DSC for K–I, 188 °C, 15.1 kcal/mol; $^1\text{H NMR}$ (CDCl_3) δ 0.90 (broad s, 12 H), 1.33 (m, 32 H), 1.49 (m, 8 H), 1.61 (m, 8 H), 1.97 (m, 8 H), 4.25 (broad s, 8 H), 7.31 (m, 8 H), 8.10 (m, 8 H), 8.96 (m, 8 H); $^{13}\text{C NMR}$ (CDCl_3) δ 14.1, 22.7, 26.2, 29.3, 29.5, 29.6, 30.5, 31.9, 68.4, 112.6, (117), 120.9, 131.8, 135.6, 150.3, 158.8; HRMS $\text{C}_{80}\text{H}_{100}\text{N}_4\text{ZnO}_4$ calcd 1244.7076, found 1244.7073; UV (CHCl_3) λ_{max} (log ϵ): 428 (5.8), 558 (4.4), 598 nm (4.0).

Liquid Crystal Characterization. The transition temperatures and enthalpy changes for all phase transitions were measured with a Perkin-Elmer DSC-7 differential scanning calorimeter and were verified with a Leitz Laborlux D cross-polarized optical microscope equipped with a hot stage and a thermocouple. Transition temperatures are reported in degrees Celsius for the crystalline-to-isotropic liquid (K–I), for the crystalline-to-liquid crystalline mesophase (K–M), and for the liquid crystal-to-isotropic liquid (M–I) phase changes.

Photocurrent Measurements. Thin films consisting of doped indium–tin oxide (ITO) float glass separated by a 1.6 μm polyimide spacer were purchased from Displaytech, Boulder, Co. or were fashioned from ITO-coated float glass (1 cm by 1.5 cm, Delta Technologies, Ltd.) as previously described.⁷ The cells were capillary filled from an isotropic melt of the porphyrin and then allowed to cool slowly. Photocurrent was generated by a focused beam from a 1000 W Xe lamp (Oriental Model 6256) passed through a 12 cm water filter. The intensity of this source at the cell surface was ca. 2.6 mW/cm². The lamp was equipped with a scanning monochromator (Oriental Model 77250). Occasional use was made of a 150 W Xe lamp (Oriental Model 7340), intensity ca. 150 mW/cm², with the same water filter.

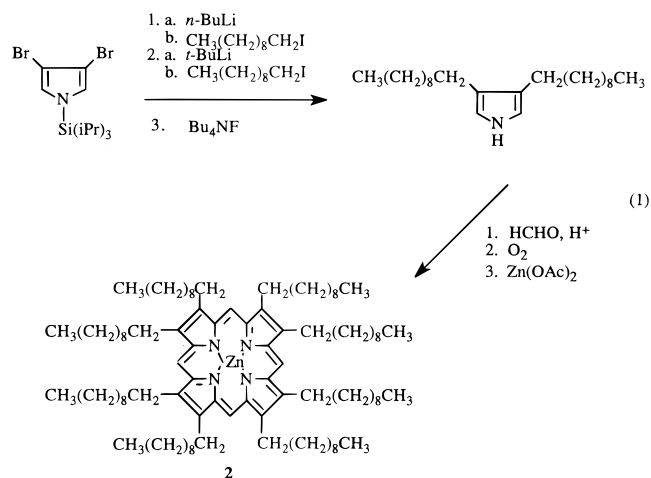
Current–voltage measurements were made with a Princeton Applied Research potentiostat (Model 173), a universal programmer (Model 175), and a current-to-voltage converter (Model 179) or on a H CH Instruments Model 660 Electrochemical Workstation. The signal was recorded by a Houston Instruments x,y -recorder (Model 1000). Action spectra were measured in an SLM Aminco SPF 500 spectrofluorometer equipped with a 250 W Xe lamp with a parabolic reflector and scanning monochromator at 2 nm resolution. The spectra were recorded by feeding the short-circuit photocurrent directly from the cell into the signal input of the spectrofluorometer and dividing out the lamp spectrum.

For time-resolved spectral measurements, the samples were excited with the second harmonic of a Nd:YAG laser (532 nm, 10 ns pulse) (Quantel YG481) under a 1.0 V applied bias, and the resulting transient photocurrents were measured and recorded in the high-resolution mode with a digitizing oscilloscope (Tektronix TDS 540, 50 Ω input impedance).^{9,15} The source of the bias was a 1.5 V battery with a variable resistor. The voltage difference between the two ITO electrodes was measured with respect to the back electrode using a voltmeter with high input impedance (Fluke 25 multimeter).

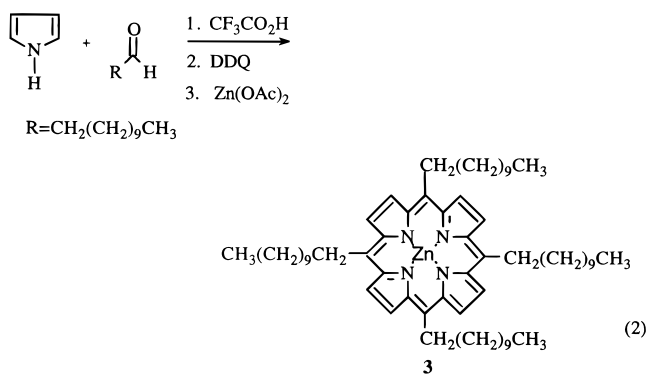
Results and Discussion

Synthesis. The synthesis of symmetrical β -substituted octaalkylporphyrins requires 3,4-disubstituted pyrroles as starting material.¹⁶ The 3- and 4-positions of 3,4-dibromo-*N*-(triisopropylsilyl)pyrrole can be selectively alkylated with high selectivity and in relatively high yield (70%).^{13,14} The resulting pyrrole was cyclized to porphyrin **2** by an acid-catalyzed condensation with formaldehyde, producing a macrocycle which was air-

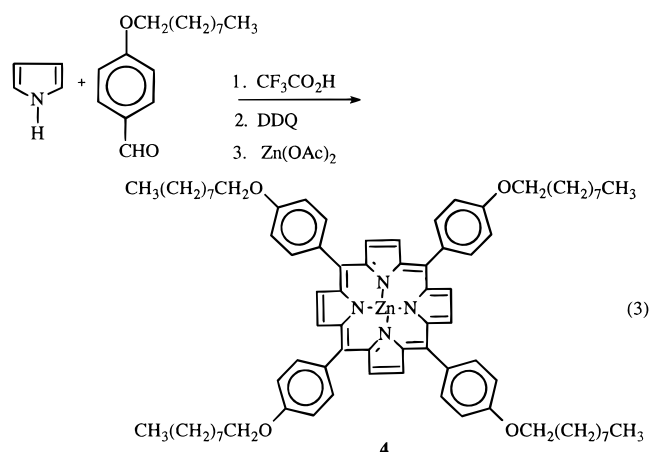
oxidized to the porphyrin (19% yield) (eq 1). The zinc complex was then obtained by metalation with $\text{Zn}(\text{OAc})_2$.



Lindsey's method¹⁷ was applied to the synthesis of porphyrins **3** and **4** with four symmetrically positioned long alkyl chains at the meso positions (eq 2). Dode-



canal condenses readily with pyrrole under high dilution conditions with acid catalysis. Upon oxidation with DDQ, the *meso*-5,10,15,20-tetra-*n*-undecylporphyrin **3** is obtained. This same procedure is also employed for porphyrin **4** with a phenyl ring between the porphyrin and the alkyl chain (eq 3).



(15) Pan, H. L.; Jones, W. E., Jr.; Melamed, D.; Fox, M. A. *J. Phys. Chem.* **1995**, *99*, 11523.

(16) Paine, J. B., III.; Kirshner, W. B.; Moskowicz, D. W.; Dolphin, D. *J. Org. Chem.* **1976**, *41*, 3857.

(17) Lindsey, J. S.; Schreiman, I. C.; Hsu, H. C.; Kearney, P. C.; Marguerettaz, A. M. *J. Org. Chem.* **1987**, *52*, 827.

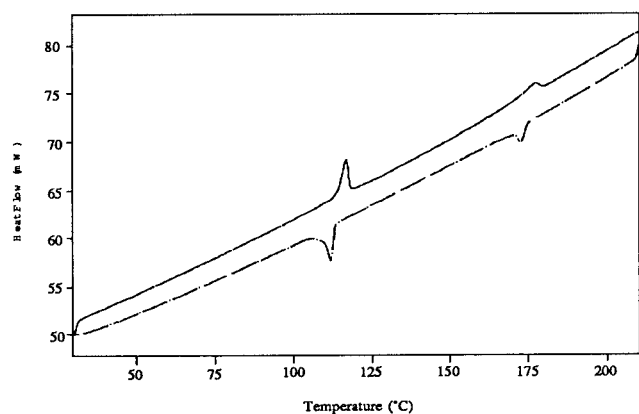


Figure 1. Differential scanning calorimetry scan for **2**. The solid line is the heating curve and the dashed line is the cooling curve. Scan rate for both curves, 5 °C/s.

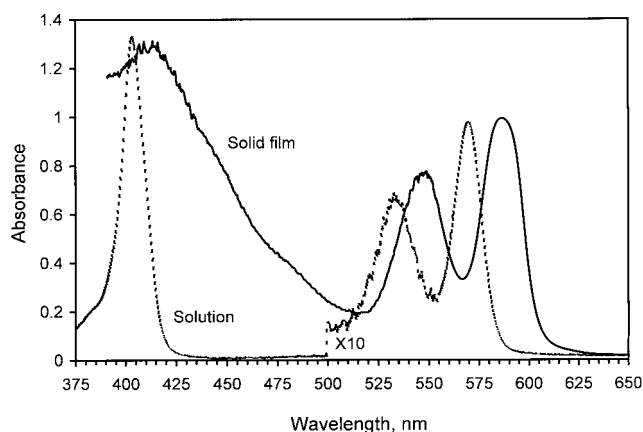


Figure 2. Solid-state and solution (CHCl₃, ca. 10⁻⁵ M) phase absorption spectra of **2**.

Phase Behavior. Differential scanning calorimetry for **2** (Figure 1) reveals two phase transitions: one at 117 °C (with a measured enthalpy of 4.5 kcal/mol), assigned as the crystalline-to-mesophase transition, and a second at 177 °C (with measured enthalpy of 2.1 kcal/mol), assigned as the mesophase-to-isotropic melt. These values are similar to those reported in the structurally analogous **1**.^{8,11} Although tetrasubstituted porphyrins can exhibit mesomorphic properties, neither **3** nor **4** display intermediate phases between the solid and the isotropic melt.

Absorption in Solution and as a Thin Film. The absorption spectra of compounds **2–4** are typical of those observed for a metalated porphyrin,^{8,18,19} exhibiting a strong Soret absorption at around 400 nm and a pair of weaker Q-bands between 500 and 600 nm. The same absorption bands are also present when these compounds are formulated as solid thin films, although the Soret band is broadened and the Q-bands shift further to the red because of the π stacking of the porphyrins in the solid phase. As shown in Figure 2 for **1** and in Figure 3 for **3** (M = Zn), normalized, solid-state spectra also show much stronger Q-band absorptions (relative to the Soret band) than in homogeneous solution, in part because of heterogeneous absorption such that light bypasses some strongly absorbing aggregates.

(18) Gregg, B. A.; Fox, M. A.; Bard, A. J. *J. Phys. Chem.* **1989**, *93*, 4227.

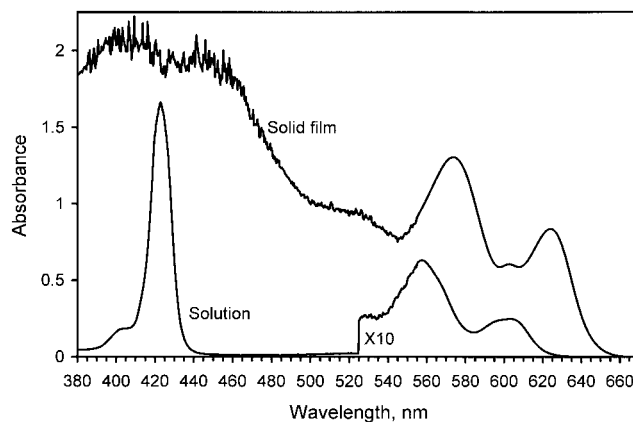


Figure 3. Solid state and solution (CHCl₃, ca. 10⁻⁵ M) phase absorption spectra of **3** (M = Zn).

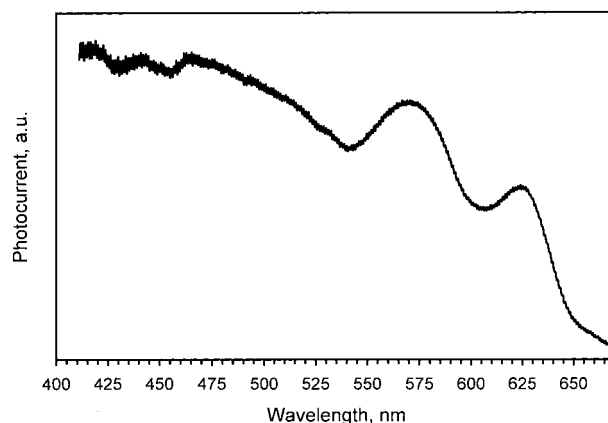


Figure 4. Solid-state absorption and photocurrent action spectra of **3** (M = Zn).

Photocurrent Measurements. When thin solid films of porphyrins **2–4** are sandwiched between conductive, optically transparent ITO plates in a solid-state photoelectrochemical cell, appreciable short circuit photocurrent and open circuit photovoltage are induced by visible light excitation, as has been described earlier for **1**.^{7–11} A strong correlation between the action spectra and the solid-state absorbance spectra is observed for very thin layers (up to ca. 1 μm)⁷ of **1–4**, as shown in Figure 4 for **3** (M = Zn). With much thicker cells, minima in the action spectra are observed at the absorbance maxima (Table 1). This has been previously attributed to potential-dependent carrier recombination,²⁰ space charge effects,²¹ or optical filtering effects.^{7,22,23} Wavelengths of light that are less strongly absorbed penetrate deeper into the cell, thereby reducing the electrical resistance through the photoconductive film, leading to higher photocurrent in thick cells and producing an inverted spectrum relative to the solid-state absorbance spectra. For thin cells, the penetration depth of a strongly absorbed wavelength represents a larger portion of the layer thickness than in a thicker cell.

(19) Smith, K. M., Ed. *Porphyrins and Metalloporphyrins*; Elsevier Scientific: New York, 1975.

(20) Kommandeur, J.; Schneider, W. G. *J. Chem. Phys.* **1958**, *28*, 582.

(21) Lyons, L. E.; Mackie, J. C. *J. Chem. Soc.* **1960**, 5186.

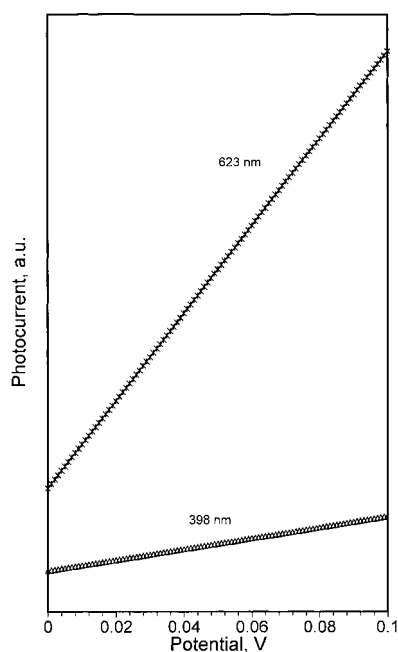
(22) Loutfy, R. O.; Hsiao, C. K.; Ho, R. *Can. J. Phys.* **1983**, *61*, 1416.

(23) Yamashita, K.; Harima, Y.; Iwashima, H. *J. Phys. Chem.* **1987**, *91*, 3055.

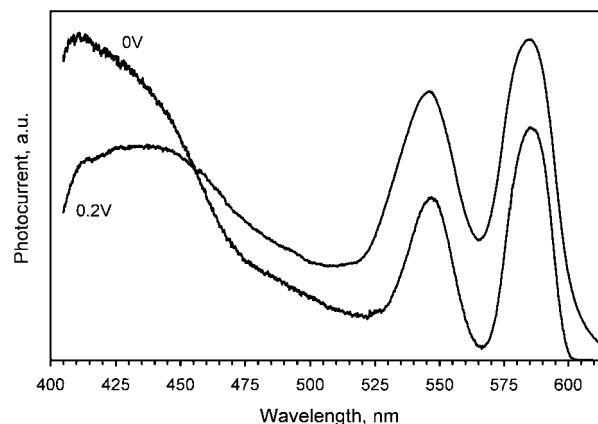
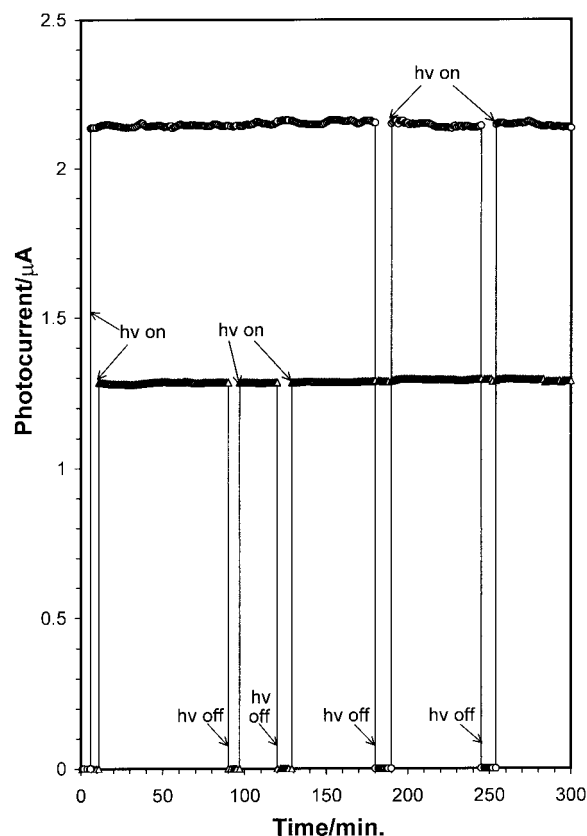
Table 1. Action and Absorption Spectra for Porphyrins 2–4 as 1.6 μm Films

compound	absorption maxima, λ_{max} (nm)		action spectra ^a	
	in soln ^b	in solid ^c	λ_{max}	λ_{min}
2	406, 536	572	413, 562, 598	540, 582
3				
M = Zn	424, 558, 602	568, 606	402, 540, 592	571, 603
M = Cu	402, 535, 595	564, 610	<i>d</i>	<i>d</i>
M = Co	414, 542 ^e	564, 610	<i>d</i>	<i>d</i>
M = Pd	420, 532, 564	542, 586	<i>d</i>	<i>d</i>
4	428, 558, 598	568, 602	422, 500, 560	551, 582

^a Measured in an ITO sandwich cell by the procedures described in the Experimental Section. ^b As 10^{-5} M solutions in EtOH. ^c As reflectance absorption spectra on thin solid films at room temperature. The Soret band overlapped significantly with ITO absorption, so apparent λ_{max} values in that region are meaningless. ^d The weak photocurrent response could not be distinguished unambiguously from incompletely filtered lamp noise. ^e The Q(0,0) band could not be detected.

**Figure 5.** Wavelength dependence of short-circuit photocurrent on externally applied bias for a 1.6 μm thick layer of **3** (M = Zn), in a solid-state thin layer photocell.

The magnitude of the observed photocurrent is linear with incident light intensity at the low light fluxes employed here, in parallel with observations made earlier for **1** and its homologues. In addition, when photocurrent is measured while applying an external bias, a linear dependence on bias potential is observed (Figure 5). In fact, although the action spectra measured at zero applied bias predict comparable photoeffects from irradiation into the Soret and Q-bands, a more sensitive response to applied bias is observed for irradiation into the Q-bands than into the Soret, as shown for **2** (M = Zn) in Figure 5. The crossover in anodic photocurrent production can be seen graphically in the action spectra observed for **2** with and without a 0.2 V bias (Figure 6). Such a result would be expected as a consequence of differential light penetration into the absorptive layer, followed by potential-dependent charge hopping toward the irradiated ITO electrode, where charge injection takes place. Since the sandwich cell is symmetrical, reversal of bias produces an additive effect.⁷

**Figure 6.** Bias-dependence of action spectra for a 1.6 μm thick layer of **3** (M = Zn) upon irradiation into the Soret and Q-bands.**Figure 7.** Prolonged measurements of steady-state short-circuit photocurrent produced upon irradiation of 1.6 μm thick cells of **2** (upper curve) and for **3** (M = Zn) (lower curve). The irradiation source was a water-filtered 1000 W Xe lamp, producing a flux of about 2.6 mW/cm² at the front face of the sandwich cell.

When a fixed light flux is employed, a very steady and reproducible photocurrent is observed, the magnitude of which depends on the identity of the light responsive porphyrin employed. As shown in Figure 7, steady-state photocurrent can be followed for hours without any appreciable loss. Listed in Table 2 are the relative magnitudes of open-circuit photovoltages and short-circuit photocurrents with and without an applied bias obtained for 1.6 μm thick layers of porphyrins **1–4**.

Several trends in these measurements are clear. First, independent of the metal or the packing of the zinc porphyrin, each thin solid layer produced photo-

Table 2. Relative Photoresponses^a Observed in 1.6 μm Thin Layers of 1–4 in an ITO Sandwich Cell

compound	V_{oc} (mV \pm 20 mV)	$j_{sc}/j_{sc}(\mathbf{1}) \pm 10\%^{b,c}$
2	200	1.0
3		
M = Zn	220	0.48
M = Cu	250	0.003
M = Co	190	0.002
M = Pd	170	0.006
4	200	0.004
1	250	1.8

^a Conditions as described in Experimental Section. ^b Normalized to the photocurrent observed for **2**. ^c Although the ratio reported here provides for a dimensionless internal comparison, the observed photocurrents were on the order of $2 \mu\text{A}/\text{cm}^2$; see Figure 7.

voltages between 150 and 250 mV. The photovoltage is thus less sensitive to structure than is the steady-state photocurrent, probably because of the comparability of the redox potentials of these families relative to the ITO band edges. Second, metalloporphyrins containing zinc produce photocurrent with much higher efficiency than do those bearing copper, cobalt, or palladium. A likely interpretation is that zinc is unique in the complexes prepared here in permitting effective charge injection from a long-lived singlet excited state of the porphyrin.¹⁹ In addition, the zinc complexes are also known to stack well, promoting effective long-range exciton migration. Third, the looser packing in **4** is associated with a steady-state photocurrent substantially lower than in **2** or **3**, (M = Zn), probably because the orthogonal *meso*-phenyl rings interfere with π stacking. Finally, porphyrin **3** (M = Zn), which lacks a stable liquid crystalline mesophase, functions nearly as well as porphyrins **1** and **2**, which do possess such a phase.

By employing flash laser excitation as the source of incident light, transient photocurrents were measured for sandwich photocells containing **2–4**.¹⁵ Two decay components, whose lifetimes were independent of the magnitude of the applied bias, were observed in each cell (Table 3) when conducted under a 1 V bias: a major (65–90%) short-lived component, with a lifetime of about 1 μs , and a minor (10–35%) longer lived component, persisting for up to tens of microseconds. This result is parallel to that described earlier for **1**, where the short component was assigned to recombination of charged carriers (trapped holes and electrons) from shallow traps and the long component was assigned to deep traps responsible for long-term charge storage. Both kinds of traps are frequently found in organic semiconductors.^{9,10} Long-term charge storage is less efficient in these materials than in **1**, suggesting that

Table 3. Transient Photocurrent Lifetimes Induced by Flash Excitation of Thin Layers of 1–3 in an ITO Sandwich Cell^{a,b}

compound	τ_1 (μs), % contribution ($\pm 0.1 \mu\text{s}$)	τ_2 (μs), % contribution
2	1.8, 66%	18 ± 5 , 34%
3		
M = Zn	4.1, 88%	140 ± 80 , 12%
M = Cu	1.0, 87%	38 ± 28 , 13%
M = Pd	0.4, 86%	2.2 ± 0.8 , 14%
4	0.4, 86%	3.1 ± 0.2 , 13%

^a Lifetimes measured with a 50 Ω input impedance with pulse excitation at 532 nm with a 10 ns pulse ($0.4 \text{ mJ}/\text{cm}^2$) under a 1.0 V applied bias. ^b Experimental variation between the decay fits could be attributed to noise within the cell and to differences between cells arising from manual fabrication.

the deep traps are less numerous in **2–4** than in **1**. These new porphyrins will therefore be less useful than **1** as materials for optoelectronic information storage.^{9,10}

Conclusions

Solid-state packing of the alkylated porphyrins described here clearly influences the attainable photoconductivity and the efficiency of photocurrent production when these materials are formulated as thin solid films in ITO sandwich cells. Porphyrin **2** exhibits a substantial photoresponse, comparable in magnitude to that of **1**. Although a stable liquid crystalline phase facilitates annealing to achieve long-range ordering, which is crucial to charge trapping in imaging applications, such a phase is not absolutely necessary for efficient photocurrent production. However, higher photoefficiencies are observed with **2** than with **3** or **4**. As had been observed with **1**, metalation of porphyrin **3** with zinc produces a higher steady-state photocurrent than with copper or cobalt, probably because zinc can promote aggregation and stacking without appreciable perturbation of partitioning of nonradiative pathways available to the singlet excited state. Transient photocurrent measurements establish two components in the decay following interfacial charge transfer, presumably corresponding to shallow and deep traps in the organic thin film.

Acknowledgment. The porphyrin syntheses were supported by the U.S. Department of Energy, Office of Basic Energy Science, and the device measurements were supported by the Texas Advanced Research Program.

CM970491V